Polythiophene–Block–Polyfluorene and Polythiophene–Block–Poly(Fluorene–co–Benzothiadiazole): Insights into the Self–Assembly of All–Conjugated Block Copolymers

ARTICLE *in* MACROMOLECULES · JANUARY 2011

Impact Factor: 5.8 · DOI: 10.1021/ma102728z

530 *Macromolecules* **2011**, *44*, 530–539
DOI: 10.1021/ma102728z

Macromolecules
ARTICLE

Polythiophene-*block*-polyfluorene and Polythiophene-*block*-poly(fluorene-*co*-benzothiadiazole): Insights into the Self-Assembly of All-Conjugated Block Copolymers

Rafael Verduzco,*,† Ioan Botiz,‡ Deanna L. Pickel,∥ S. Michael Kilbey II,∥,⊥ Kunlun Hong,∥ Elaine Dimasi,§ and Seth B. Darling*,‡

†*Department of Chemical and Biomolecular Engineering, Rice University, 6100 Main Street, MS-362, Houston, Texas 77005, United States,* ‡*Center for Nanoscale Materials, Argonne National Laboratory, 9700 South Cass Avenue, Argonne, Illinois 60439, United States,* ∥*Center for Nanophase Materials Sciences, Oak Ridge National Laboratory, One Bethel Valley Road, Oak Ridge, Tennessee 37831, United States,* ⊥*Department of Chemistry, University of Tennessee, Knoxville, Tennessee 37996, United States, and* §*National Synchrotron Light Source, Brookhaven National Laboratory, Upton New York 11973, United States*

Received November 30, 2010; Revised Manuscript Received December 7, 2010

ABSTRACT: All-conjugated block copolymers have significant potential for solution-processed optoelectronic applications, in particular those relying on a p/n junction. Herein, we report the synthesis and structure of all-conjugated diblock copolymers poly(3-hexylthiophene)-*block*-poly(9,9-dioctylfluorene) and poly(3-hexylthiophene)-*block*-poly(9,9-dioctylfluorene-*co*-benzothiadiazole) in thin films and in the bulk. The diblock copolymers are prepared using a combination of Grignard metathesis polymerization and Suzuki polycondensation and characterized with NMR spectroscopy, size-exclusion chromatography, multiangle laser light scattering, and UV/vis spectroscopy. Structure in thin films and in the bulk is characterized using differential scanning calorimetry, X-ray diffraction, small-angle X-ray scattering, and atomic force microscopy. Diblock copolymer thin films self-assemble into a crystalline nanostructure with some long-range order after extended solvent annealing, and X-ray scattering measurements show that powder samples exhibit crystallinity throughout the bulk. By temperature dependent X-ray scattering measurements, we find that diblock copolymers self-assemble into crystalline nanowires with phase segregated block copolymer domains. These measurements show all-conjugated diblock copolymers may be useful for achieving solution-processed active layers in organic photovoltaics and light-emitting diodes with optimized structural and photophysical characteristics.

Introduction

Semiconducting polymers (also known as π-conjugated or simply conjugated polymers) combine the optical and electronic properties of semiconductors with the processing advantages of polymers. Because of the extended π-conjugated backbone (e.g., alternating double and single bonds), these polymers exhibit photophysical properties characteristic of inorganic semiconductors, including a finite energy bandgap and fluorescence. The rigid, π-conjugated backbone generally leads to decreased solubility in common organic and aqueous solvents, but incorporation of side chains into conjugated polymers improves their solubility and enables solution processing for thin-film, large-area device applications.[1] A number of potentially revolutionary technologies based on conjugated polymers have been proposed, including organic photovoltaics (OPVs),[1,2] thin-film transistors,[3] white organic light-emitting diodes,[4] and fluorescent chemical sensors.[5]

Many applications of organic semiconductors require two distinct semiconductors with different charge transport properties and energy bandgaps. OPVs and organic light-emitting diodes (OLEDs) in particular show improved performance when a p-type, or hole-transporting, component is combined with an n-type, or electron-transporting, component.[6] In OPVs, this can be achieved by solution blending a p-type conjugated polymer with an n-type fullerene derivative followed by solvent casting and annealing to create what is known as a bulk-heterojunction (BHJ) active layer.[7] The polymer and fullerene phase separate during the solvent casting and annealing process, resulting in an active layer with nanoscale p- and n-type domains with sizes that are correlated with relatively efficient exciton separation and charge transport. BHJ OPVs are currently the best performing polymer-based PVs, but efficiencies are still lower than expected for an optimized OPV device;[8,9] it is widely accepted that the nanoscale morphology of the active layer plays a critical role in determining the efficiency of the processes underlying photon-to-electricity conversion. Controlling the active layer morphology in BHJ OPVs is a major challenge because the final structure depends on processing conditions, including the choice of the casting solvent, annealing time and temperature, composition, and solution concentration.[10] New materials and/or processing methods that can reliably generate well-defined p- and n-type domains would facilitate investigation—and ultimately optimization—of the active layer structure for OPV devices or for multilayer constructs needed for polymer OLED devices.[4,11]

The use of block copolymers (BCPs) can potentially address these challenges because they can spontaneously self-assemble into regular nanostructures under a variety of processing conditions and environments.[12−14] As suggested in recent reviews,[15−18]

*Corresponding authors. E-mail: (R.V.) rafaelv@rice.edu; (S.B.D.) darling@anl.gov.

 Published on Web 01/10/2011

self-assembly of all-conjugated BCPs may be particularly useful for achieving solution-processed active layers in OPVs and OLEDs with optimized structural and photophysical characteristics. Extensive work with BCPs has yet to produce an OPV or OLED that performs as well as polymer-fullerene devices, but the vast majority of this work has focused on BCPs where one or both polymer blocks is not conjugated. Conjugated polymers show the best performance in organic electronic applications, and all-conjugated BCPs can potentially act as both structure-directing agents as well as active components in a device. Furthermore, recent work suggests that all-conjugated BCPs can improve the performance of all-polymer OPV[19] and OLED[20] devices, and conjugated polymer blends have shown promising performance in OPVs.[21−30]

Conjugated polymers are typically synthesized by condensation and cross-coupling reactions, which give poor control over molecular weight, polydispersity (PDI), and end-group functionality. However, recent efforts have provided new methods for the synthesis of all-conjugated BCPs.[31] Grignard metathesis (GRIM) polymerization is a versatile method for making poly(3-alkylthiophenes) with targeted molecular weights, PDIs less than 1.2, and high regioregularity.[32] Several all-conjugated BCPs have also been synthesized by GRIM polymerization.[33−38] These polymers are based almost exclusively on a thiophene repeat unit and are typically p-type, but donor/acceptor block polymers can be made by functionalization of the polythiophene backbone with a variety of side-chains.[39,40] GRIM polymerization can also be used to prepare polyfluorene homopolymers and BCPs of polythiophene and polyfluorene.[41,42] Using a different approach that involves GRIM and Suzuki polymerization reactions, Scherf et al. reported the synthesis of polythiophene-*block*-polyfluorene copolymers that can self-assemble in thin films and at the air−water interface.[43,44] Currently, the only report of an OPV device based on an all-conjugated BCP is provided by Sun et al.[19] Other reports on all-conjugated BCPs have produced materials for white OLEDS[20] as well as other applications,[45] as detailed in recent reviews.[15−18,31]

While these studies have established novel synthetic routes to all-conjugated BCPs, much of the previous work has involved all-conjugated BCPs that contain two p-type polymers or wide-bandgap polymers not suitable for OPVs. Furthermore, the self-assembly of all-conjugated polymers is poorly understood and oftentimes characterized using only AFM imaging, which does not address the morphological structure throughout the bulk of polymer films. Also, all-conjugated BCPs are often not fully characterized with respect to the absolute molecular weight and the presence of homopolymer impurities. These factors underscore the considerable need for fundamental studies involving well-made, rigorously characterized all-conjugated BCPs and their self-assembly. Herein, we report the synthesis and characterization of two all conjugated diblock copolymers: poly(3-hexylthiophene)-*block*-poly(9,9-dioctylfluorene) and poly(3-hexylthiophene)-*block*-poly(9,9-dioctylfluorene-*co*-benzothiadiazole). These polymers are synthesized using a combination of GRIM and Suzuki polymerizations and characterized with a combination of NMR spectroscopy, size-exclusion chromatography (SEC), multiangle laser light scattering (MALLS), and UV/vis spectroscopy. We present a method for quantifying the amount of homopolymer impurities in all-conjugated block copolymer samples. The structure and thermal properties of thin film and polymer melt samples are investigated using differential scanning calorimetry (DSC), X-ray diffraction (XRD), atomic force microscopy (AFM), and small-angle X-ray scattering (SAXS). We find that all-conjugated diblock copolymers can self-assemble into periodic crystalline nanostructures in thin films and in bulk powder samples.

Experimental Section

Materials. 9,9-Dioctyl-2,7-dibromofluorene, 4,7-dibromobenzo[1,2,5]thiadiazole, 9,9-dioctylfluorene-2,7-diboronic acid bis(1,3-propanediol) ester, Aliquat 336, tetrakis-(triphenylphosphine)palladium(0), and sodium carbonate (Na_2CO_3) were purchased from Aldrich and used as received. Anhydrous THF (Drisolve), chloroform, diethyl ether, methanol, hexanes, ethyl acetate, dichloromethane, and toluene were purchased from VWR and used as received. Bromo-terminated poly(3-hexylthiophene) (P3HT-Br)[34] and 7′-bromo-9′,9′-dioctylfluoren-2′-yl-4,4,5,5-tetramethyl[1,3,2]dioxaborolane[46] were synthesized as previously described.

Poly(3-hexylthiophene)-*b*-poly(9,9-dioctylfluorene) (P3HT-*b*-PFO). P3HT-Br (505 mg, 0.051 mmol), 7′-bromo-9′,9′-dioctylfluoren-2′-yl-4,4,5,5-tetramethyl[1,3,2]dioxaborolane (1.75 mg, 2.94 mmol), 1−2 drops of Aliquat 336, and tetrakis(triphenylphosphino)palladium(0) (123 mg, 0.108 mmol), 40 mL of toluene, and 20 mL of 2 M aqueous Na_2CO_3 were combined in a Schlenk tube, degassed by three freeze−pump−thaw cycles, and backfilled with nitrogen. The reaction was carried out at 85 °C for 72 h, after which the reaction was cooled to room temperature and precipitated into 200 mL of cold methanol. The product was recovered by filtration, loaded into a Soxhlet thimble, and washed with methanol (2 h), diethyl ether (2 h), and hexanes (7 h) to remove poly(9,9-dioctylfluorene) homopolymer and other small molecule impurities. The polymer was further purified by silica gel column chromatography to remove unreacted P3HT-Br using 90% toluene and 10% acetonitrile (v/v) as the eluent. ^{1}H NMR (500 MHz, $CDCl_3$): δ 7.5−8.0 (m, 1.5 H), 6.9−7.0 (s, 1.0 H), 2.7−2.9 (s, 2.0 H), 2.0−2.3 (m, 1.0 H), 0.7−1.7 (m). ^{13}C NMR (100 MHz, CDCl3): δ 150.8, 138.6, 132.7, 129.5, 127.8, 125.0, 122.0, 120.5, 119.0 54.3, 39.4, 30.8, 30.7, 29.5, 28.7, 22.9, 21.6, 13. SEC−RI/MALLS: dn/dc = 0.226, M_w = 16 700 g/mol, PDI = 1.31.

Poly(3-hexylthiophene)-*b*-poly[(9,9-dioctylfluorene)-*co*-(2,3,5-benzothiadiazole)] (P3HT-*b*-PFBT). P3HT-Br (386 mg, 0.039 mmol), 9,9-dioctyl-2,7-dibromofluorene (541 mg, 0.99 mmol), 4,7-dibromobenzo[1,2,5]thiadiazole (75 mg, 0.25 mmol), 9,9-dioctylfluorene-2,7-diboronic acid bis-(1,3-propanediol) ester (690 mg, 1.24 mmol), 1−2 drops of Aliquat 336, and tetrakis(triphenylphosphino)palladium-(0) (103 mg, 0.090 mmol), 30 mL of toluene, and 15 mL of 2 M aqueous Na_2CO_3 were combined in a Schlenk tube, degassed by three freeze−pump−thaw cycles, and backfilled with argon. As before, the reaction was carried out at 85 °C for 72 h, after which the reaction was cooled to room temperature and precipitated into 200 mL of cold methanol, recovered by filtration, and then loaded into a Soxhlet thimble and washed with methanol (2 h), diethyl ether (2 h), and hexanes (7 h) to remove PFO homopolymer and small molecule impurities. The polymer was further purified by silica gel column chromatography to remove unreacted P3HT-Br using 90% toluene and 10% acetonitrile as the eluent. While this synthesis can produce triblock copolymers in addition to the desired diblock copolymers, the proportion of triblock copolymers is insignificant due to the low molar content and relatively low reactivity of P3HT-Br. ^{1}H NMR (400 MHz, $CDCl_3$): δ 7.4−8.0 (m, 4.7 H), 6.95−7.0 (s, 1.0 H), 2.7−2.9 (t, 1.9 H), 1.9−2.3 (m, 2.6 H), 0.7−1.7 (m). ^{13}C NMR (100 MHz, CDCl3): δ 151.8, 139.9, 133.7, 130.5, 128.6, 126.2, 121.5, 120.0, 55.4, 40.4, 31.8, 30.5, 30.3, 30.0, 29.7, 29.3, 23.4, 22.7, 14.1. SEC−RI/MALLS: dn/dc = 0.242, M_w = 18 900 g/mol, PDI = 1.43.

Instrumentation. *Nuclear Magnetic Resonance Spectroscopy* (*NMR*). Solution ^{1}H NMR and ^{13}C NMR (d_1 = 5 s)

Scheme 1. Synthetic Scheme for the Preparation of All-Conjugated Rod−Rod Copolymers Poly(3-hexylthiophene)-*block*-poly(9,9-dioctylfluorene) (P3HT-*b*-PFO) and Poly(3-hexylthiophene)-*block*-poly(9,9-dioctylfluorene-*co*-benzothiadiazole) (P3HT-*b*-PFBT)

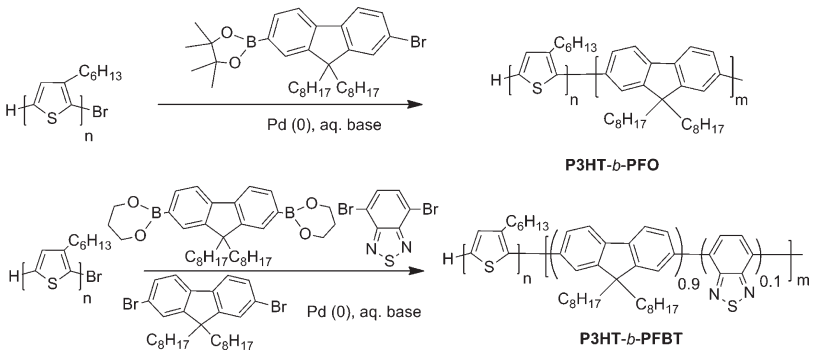

spectroscopy was performed on a Bruker 400 MHz multinuclear spectrometer. Samples were placed in 5 mm o.d. tubes with sample concentrations of 10 and 20% (w/v), respectively. Chloroform-*d* ($CDCl_3$, Cambridge Isotope) was used as the solvent with TMS (0.1%) as an internal standard.

Size-Exclusion Chromatography (*SEC*). Molecular weights and polydispersities were obtained by SEC using an Agilent 1200 module equipped with three PSS SDV columns in series (100, 1000, and 10 000 Å pore sizes), an Agilent variable wavelength UV/visible detector, a Wyatt Technology HELEOS II multiangle laser light scattering (MALLS) detector (λ = 658 nm), and a Wyatt Technology Optilab reX RI detector. This system enables SEC with simultaneous refractive index (SEC−RI), UV/vis (SEC−UV/vis), and MALLS detection. THF was used as the mobile phase at a flow rate of 1 mL/min at 40 °C. Absolute molecular weights are determined by light scattering with dn/dc values calculated using the RI detector and assuming 100% mass recovery of the injected sample (Astra Software Version 5.3.4).

Atomic Force Microscopy (*AFM*). Tapping-mode AFM imaging was performed using a Veeco MultiMode V scanning probe microscope equipped with acoustic and active vibration isolation. Etched silicon probes with force constants of ~40 N/m were used to acquire all images. Both phase-and height-modulated images were obtained. Height-modulated AFM measures changes in the amplitude of oscillation of the AFM cantilever while phase-modulated AFM measures the difference between the driven and the actual oscillations of the cantilever.[47]

X-ray Diffraction (XRD). X-ray diffraction data were obtained using a Bruker D8 Discover analytical X-ray system in a grazing incidence geometry (θ_i = 0.18).

Differential Scanning Calorimetry (*DSC*). Differential scanning calorimetry measurements were performed using a Mettler-Toledo DSC 823^e with a ramp rate of 10 °C/min.

Small-angle X-ray Scattering (*SAXS*). X-ray scattering experiments were performed at beamline X6B at the National Synchrotron Light Source at Brookhaven National Laboratory. Samples in powder form were loaded into 1.0 mm thick glass capillaries and inserted into aluminum cassettes which had a 1.5 mm hole with ±15 degrees of angular range for SAXS measurements. The cassettes fit into a standard hot stage (Instec model HCS402) with a temperature stability of approximately 0.1 °C. The hot stage containing the sample cassette was mounted in a vacuum chamber and centered in an evacuated flight path on the beamline. The incident beam energy was set to 16 keV (wavelength λ = 0.775 Å and energy resolution $\Delta E/E = 10^{-4}$) or 8 keV (wavelength λ = 1.55 Å and energy resolution $\Delta E/E = 10^{-4}$); the beam cross-section was reduced to 0.2 mm horizontal ×0.3 mm vertical by slits placed 1 m upstream of the sample. Two dimensional SAXS images were recorded by a Princeton Instruments CCD area detector (2084 × 2084 array with 116 mm wide active area) located approximately 1.2 m from the sample. The correspondence between CCD pixel position on the detector and scattering wavenumber q was determined by calibration using a standard silver behenate powder placed at the sample position. The effective q resolution of the apparatus was 0.0033 $Å^{-1}$. SAXS measurements were carried out on powder samples that were heated to 250 °C, which is above the crystallization temperature for all samples studied and therefore erases the thermal history of the samples. Samples were held at each temperature for 2 min for measurement, and SAXS patterns were acquired in 5 °C increments with a 5 min thermal equilibration at each temperature before measurement.

Results and Discussion

Synthesis of All-Conjugated Diblock Copolymers. The target BCPs chosen for this study are composed of poly(3-hexylthiophene) (P3HT) as the p-type block and a polyfluorene-based polymer as the n-type block (Scheme 1). P3HT is one of the most widely studied and best performing polymers in BHJ OPVs, serving as a benchmark material because it can be synthesized with controlled molecular weight, polydispersity less than 1.2, controlled end-group functionality, and high regioregularity.[32] Poly(9,9-dioctylfluorene) (PFO) is a wide bandgap polymer with good photoluminescence for OLEDs, and a variety of comonomers can be incorporated to reduce the bandgap for OPV applications. In particular, poly(9,9-dioctylfluorene-*co*-benzothiadiazole) (PFBT) has good electron mobility, a moderate energy bandgap, and HOMO and LUMO levels lower than those of P3HT.[48−50] Furthermore, PFBT and other fluorene-based copolymers have shown promising results in all-polymer OPVs,[28,29] including as an n-type material in combination with P3HT.[22,27,30] Here, we focus on PFBT with just 10% benzothiadiazole units which has been shown to have electronic properties comparable to the PFBT alternating copolymer[48] (i.e., 50% benzothiadiazole units) and which we expect will exhibit improved solubility due to increased 9,9-dioctylfluorene content.

As shown in Scheme 1, our overall synthetic strategy involves a Suzuki polymerization for the synthesis of a PFO or PFBT polymer block in the presence of a polythiophene macroreagent. The P3HT macroreagent was synthesized by GRIM polymerization,[34] and the same P3HT macroreagent was used to make two different diblock copolymers. This synthetic procedure is similar to that reported recently by Tu et al.,[44] but additional purification and analysis are carried out to remove homopolymer impurities and quantify the purity of the final diblock copolymer. Homopolymer

Table 1. Summary of Polymer Characteristics As Determined by SEC and NMR

polymer	MW[a]	PDI[b]	mole ratio[c] NMR	mass ratio[c] MALLS	mole ratio[c] MALLS
P3HT	9.9	1.1			
PFO	4.9	1.6			
PFBT	3.4	2.9			
P3HT-*b*-PFO	16.7	1.3	4.0	1.5	3.5
P3HT-*b*-PFBT	18.9	1.4	1.7	1.1	2.4

[a] kg/mol, as determined by MALLS. [b] Determined via SEC−RI calibration curve based on monodisperse polystyrene standards. [c] The mole and mass ratios correspond to P3HT relative to PFO or PFBT blocks in the diblock copolymers. Using ^{1}H NMR, the degree of polymerization (DP) and mass ratios are determined by comparing the integrated intensity of the aromatic P3HT peak (6.9 ppm) to the alkyl PFO or PFBT peaks at approximately 2.2 ppm. Using MALLS, the mass and mole ratios are determined by comparing the MW of the diblock copolymers to P3HT macroreagent.

impurities are removed by a combination of solvent extraction and column chromatography. PFO and PFBT homopolymers are soluble in refluxing hexanes, and extensive washing of the polymeric product with hexanes in a Soxhlet apparatus removed PFO and PFBT homopolymer without dissolving the diblocks. Silica gel column chromatography removes unreacted P3HT macroreagent. For comparison, PFO and PFBT homopolymers were synthesized using the same reaction conditions but without P3HT macroreagent (Table 1). Both were purified by washing with methanol and acetone in a Soxhlet apparatus to remove small molecule and then hexanes to recover the polymeric product. Similar materials can be synthesized using GRIM polymerization for both polymer blocks,[41,42] but the purity of the block copolymers produced using an all-GRIM method has not been quantified. Furthermore, an all-GRIM approach may not be applicable to the preparation of random and alternating copolymers such as PFBT using commercially available materials.

SEC−RI shows an increase in molecular weight for the BCPs compared with the starting P3HT macroreagent (Figure 1). A broadening of the molecular weight distribution was observed for the diblock copolymers, which is consistent with the behaviors observed for the PFO and PFBT homopolymers; Suzuki condensation polymerizations result in broader PDI materials. The absolute molecular weight of the polymers was determined using MALLS. The MALLS detector operates at a wavelength of 658 nm, which is beyond the range of solution absorbance for both polymer blocks. In both cases, chain-extension of the P3HT block to make P3HT-*b*-PFO and P3HT-*b*-PFBT resulted in an increase in molecular weight, as seen in Table 1 and in Figure 1. The shift in the peak molecular weight in SEC−RI traces indicates that diblocks are the major product, and the presence of polymeric byproducts can be quantified, as discussed in the following paragraphs.

^{1}H NMR was used to determine the composition of the diblock copolymers by integration of peaks characteristic of PFO, PFBT, and P3HT (Figure 2 and Supporting Information). In particular, the aromatic peaks corresponding to P3HT (6.9 ppm) as well as the aliphatic peaks corresponding to $-CH_2-$ in the alkyl side chains of PFO and PFBT (2.2 ppm) are clearly resolved. These integrated intensities can be used to estimate the mole ratio of each component in the diblock copolymers after purification, and the results are given in Table 1. Comparison to the results obtained from MALLS shows fairly good agreement. ^{1}H NMR also indicates that benzothiadiazole monomer is

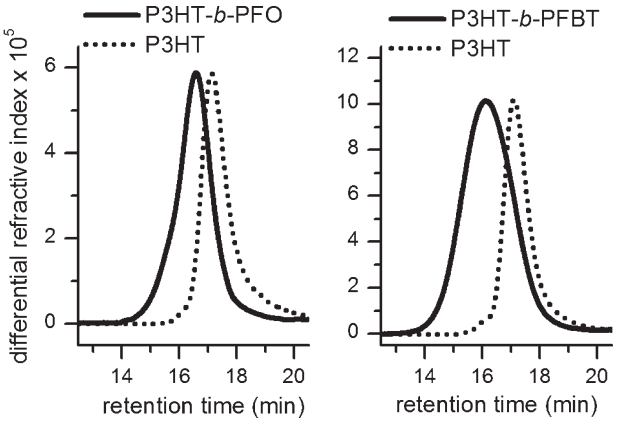

Figure 1. SEC−RI traces of P3HT-*b*-PFO (left) and P3HT-*b*-PFBT (right) block copolymers in comparison to P3HT macroreagent. Both copolymers show an increase in molecular weight relative to the P3HT macroreagent.

incorporated into P3HT-*b*-PFBT at the expected 10% molar content. First, PFBT aromatic peaks at 7.4−8.2 ppm are downshifted relative to the aromatic peaks for PFO, proving that benzothiadiazole is incorporated into PFBT and P3HT-*b*-PFBT (see Figure 2 and Supporting Information). Furthermore, the ratio of the peak intensity at 2.2 ppm to that at 7.4−8.2 ppm is 0.54 in P3HT-*b*-PFBT, close to the expected ratio of 0.59 for 10% benzothiadiazole incorporation, compared with 0.67 for P3HT-*b*-PFO. These ratios also match what is observed in the corresponding homopolymers (see Supporting Information).

To determine the amount of homopolymer impurity in the purified diblock copolymers, UV/vis spectroscopy was utilized. The absorbance of the diblock copolymers is treated as a superposition of the corresponding homopolymers, with P3HT showing maximum absorbance at 450 nm and PFO and PFBT at roughly 380 nm (Figure 3). PFO does not show any absorbance at 450 nm while PFBT shows some absorbance at 450 nm. On the basis of this, the traces at 450 and 380 nm from the UV/vis detector on the SEC system should appear qualitatively similar for diblock copolymer samples with little or no homopolymer impurity. As shown in Figure 4, the absorbance traces at 450 and 380 nm are similar in the case of P3HT-*b*-PFO but different in the case of P3HT-*b*-PFBT, suggesting a greater amount of P3HT impurity is present in the latter.

In order to quantify the amount of P3HT homopolymer impurity, solution UV/vis measurements are compared to SEC−UV/vis measurements. The ratio of the absorbance at 450 nm to that at 380 nm provides a measure of the amount of P3HT present in the mixture. It is assumed that absorbances corresponding to the peak in SEC−UV/vis elution traces reflect only diblock copolymers because absorbances due to homopolymer are observed at lower retention times relative to the diblock copolymer. On the other hand, the absorbance obtained from solution UV/vis measurements accounts for all species present in the mixture, including diblock and homopolymer. Therefore, the increase in the ratio of the absorbance at 450 and 380 nm in the solution UV/vis measurements compared with SEC−UV/vis measurements is due to the presence of P3HT homopolymer. The absorbance ratios can be related to the mass fractions of each polymer block and of P3HT homopolymers as follows: $R_{solution}/R_{sec} = (w_{P3HT}^{BCP} + w_{P3HT}^{homopolymer})/w_{P3HT}^{BCP}$, where $R_{solution}$ and R_{SEC} are the absorbance ratios in standard solution measurements and in the SEC−UV/vis measurement, respectively, w_{P3HT}^{BCP} is the mass fraction of P3HT in the diblock

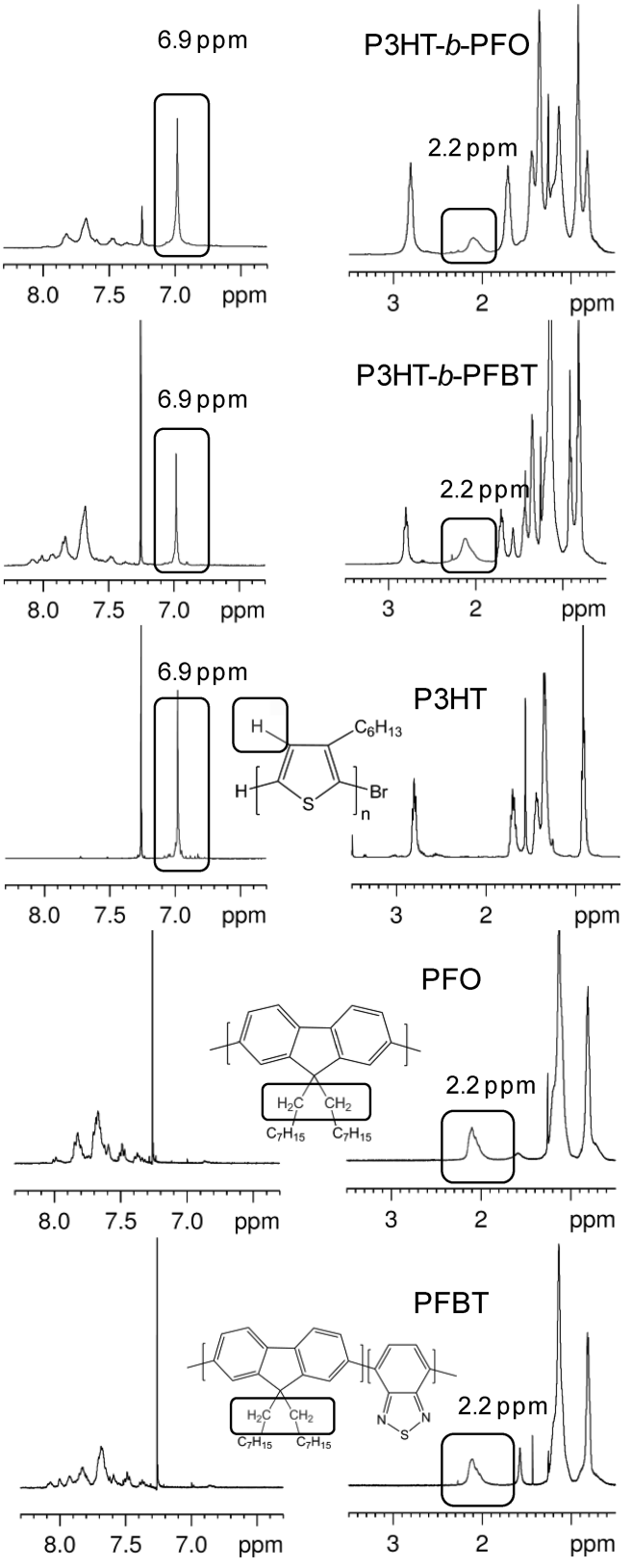

Figure 2. ^{1}H NMR spectra for conjugated block copolymers and homopolymers. The regions highlighted were used to determine the relative mole fractions of each polymer block.

copolymer, and $w_{P3HT}^{homopolymer}$ is the mass fraction of P3HT homopolymer relative to the total mass of diblock copolymer (see Supporting Information for a detailed derivation). SEC−UV/vis measurements give absorbance ratios of 0.81

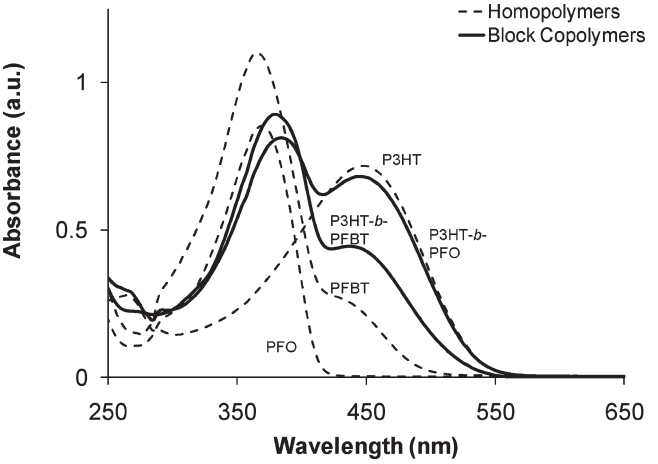

Figure 3. UV/vis absorbance measurements of block copolymers in THF. The absorbance data shows that P3HT absorbs more strongly at 450 nm compared with PFO and PFBT. On the other hand, absorbance at 380 nm is more significant in PFBT and PFO compared with P3HT.

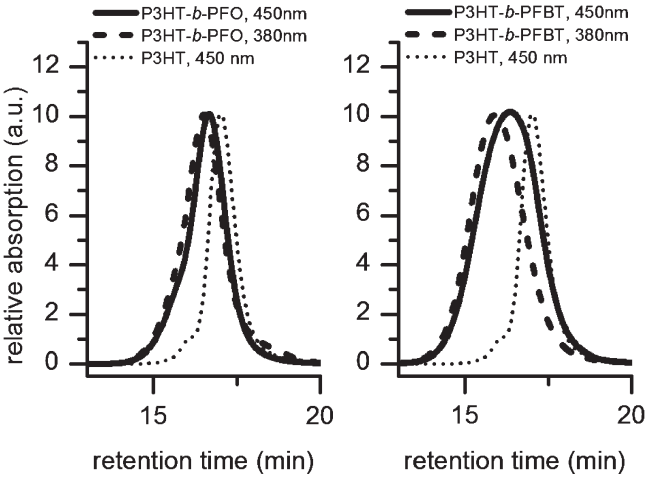

Figure 4. SEC−UV/vis traces for P3HT-*b*-PFO and P3HT-*b*-PFBT compared with P3HT macroreagent. The SEC−UV/vis traces are normalized for clarity.

and 0.38 for P3HT-*b*-PFO and P3HT-*b*-PFBT, respectively. By comparison, solution UV/vis measurements give ratios of 0.84 and 0.48 for P3HT-*b*-PFO and P3HT-*b*-PFBT, respectively. As expected, the ratios are larger in the standard solution measurements due to the presence P3HT homopolymer impurity. The relationship above and the compositions in Table 1 give an estimate of 2% and 17% P3HT homopolymer impurity ($w_{P3HT}^{homopolymer}$) in P3HT-*b*-PFO and P3HT-*b*-PFBT, respectively. Quantifying the amount of homopolymer impurity is important when interpreting physical behaviors, including the morphology of rod−rod copolymers. This has been neglected in many previous reports on all-conjugated block copolymers, and the method presented here can be applied to all-conjugated BCPs in which the conjugated polymer blocks have different absorbance properties.

As shown in Figure 5, DSC measurements of diblock copolymer samples show a thermal transition near 200 °C, where a crystal melting transition is observed for P3HT.[51] In the case of the diblocks, the peak is broad and contains multiple peaks, indicating that P3HT crystallization and other structural changes may be occurring near 200 °C. PFO shows a broad crystallization peak below 100 °C

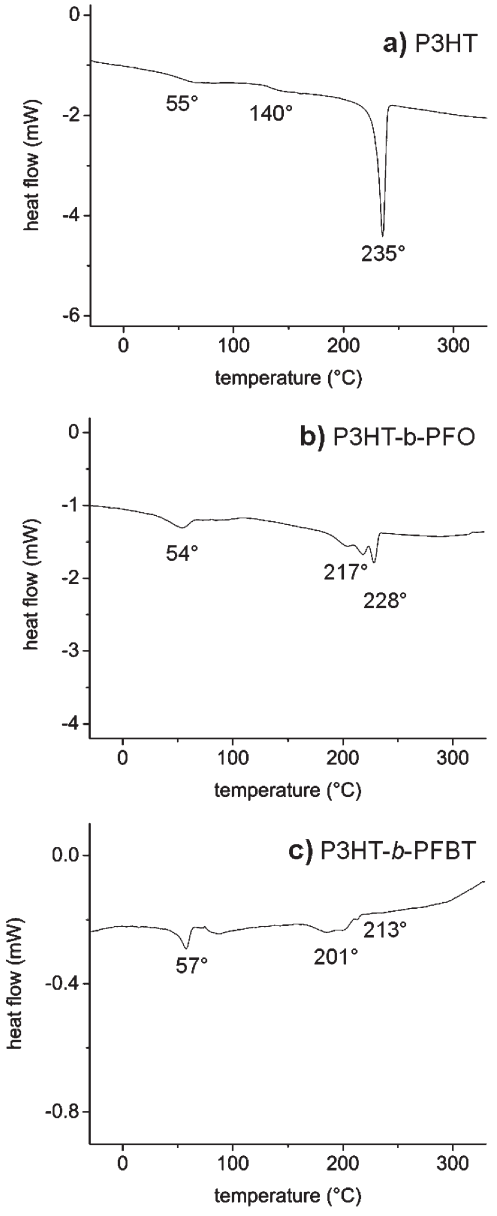

Figure 5. Differential scanning calorimetry data on second heating for (a) P3HT, (b) P3HT-*b*-PFO, and (c) P3HT-*b*-PFBT.

(see Supporting Information), but no comparable peaks are seen in the diblocks. All polymers also show a T_g near 50 °C.

Properties of All-Conjugated Diblock Copolymer Thin Films. In order to study the structure of these polymers in thin films, the polymers were spin-cast onto SiO_2 substrates, solvent annealed in dichlorobenzene at 150 °C, and characterized using XRD and AFM. The XRD data for the diblock copolymers and P3HT homopolymer presented in Figure 6 show peaks corresponding to a crystalline, lamellar morphology. The peak at $2\theta \approx 5.6°$ corresponds to an interlayer *d*-spacing of 16.36 Å, and the other two diffraction peaks at 2θ of approximately 11° and 15.8° represent second and third-order reflections of the lamellae. These values are close to those reported for P3HT thin films[52] and correspond to crystalline P3HT lamellae oriented parallel to the substrate. No diffraction peaks associated with PFO[53] are observed for the P3HT-*b*-PFO diblock copolymer thin films, which indicates that the crystallization of PFO block is suppressed in the diblock copolymer thin films. This may be due to the lower crystallization temperature of PFO or the lower degree

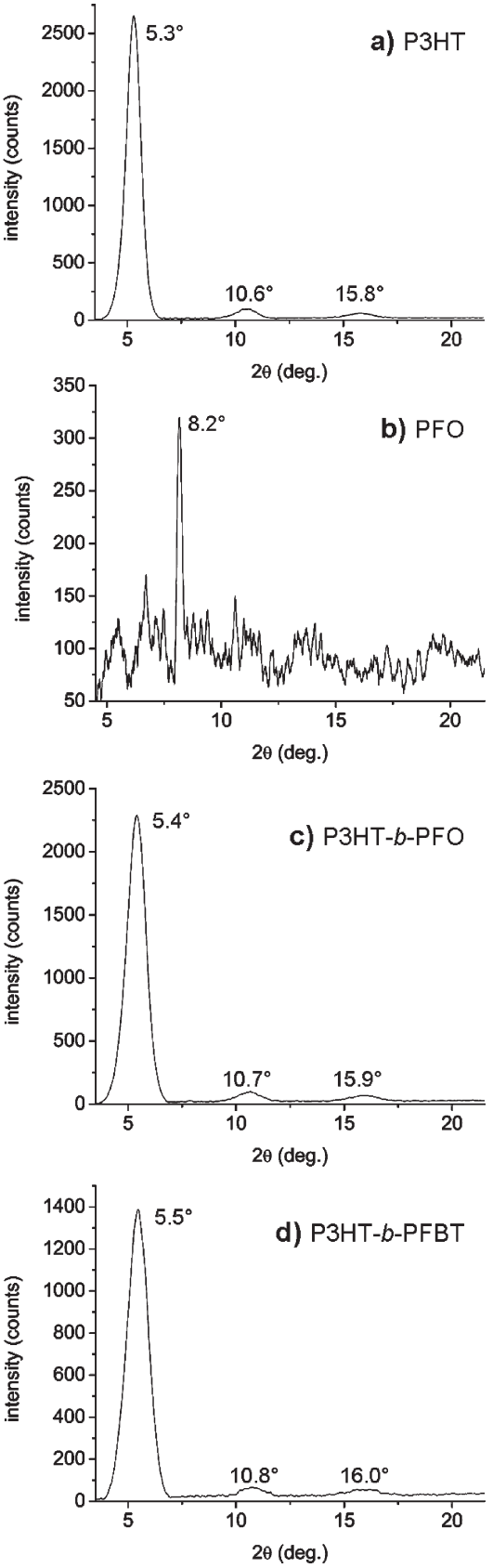

Figure 6. XRD traces for (a) P3HT, (b) PFO, (c) P3HT-*b*-PFO, and (d) P3HT-*b*-PFBT thin films spin-cast in chlorobenzene and annealed at 150 °C for 3 h.

of crystallinity of PFO, as indicated by the much weaker peak intensity observed for PFO thin films. These data suggest that

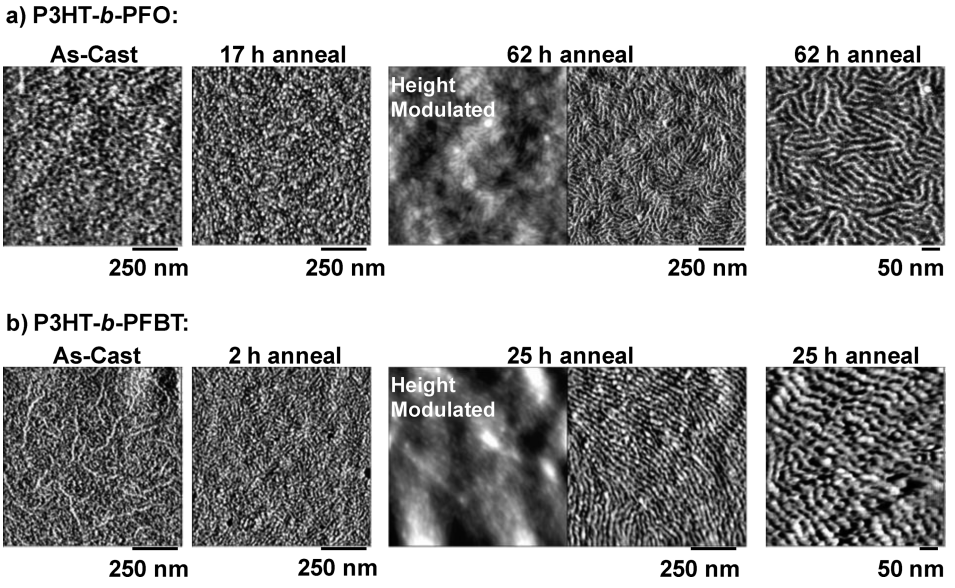

Figure 7. Atomic force microscopy images of all-conjugated block copolymer films on SiO_2. All images are obtained by phase modulation except where otherwise noted. Polymer films were solvent annealed with dichlorobenzene at 150 °C for the time shown.

the P3HT block in diblock copolymer films has a crystalline structure similar to that in P3HT homopolymer thin films. The covalent attachment of a crystalline PFO or amorphous PFBT polymer block has little or no impact on the crystallinity of the P3HT block in the diblocks. Furthermore, the suppression of PFO crystallinity may be due to limited mobility of the polymer chains after crystallization of the P3HT block. Similar behavior has been observed in related diblock copolymers with a P3HT polymer block, including both rod−coil[54,55] and rod−rod[36,56] diblocks.

AFM images show that diblock copolymer thin films develop a periodic nanostructure with some long-range order after extended solvent annealing (Figure 7). The periodic lateral nanostructure is evident in phase modulated AFM images, whereas height modulated AFM images exhibit significantly lower contrast for both P3HT-*b*-PFO and P3HT-*b*-PFBT. The formation of nanostructured domains requires long annealing times in the presence of a solvent, which may be due to the slow dynamics associated with the reorganization of a semicrystalline diblock copolymer. The width of the nanostructures is approximately 20 nm with some degree of long-range ordering, up to approximately 100 nm, and the morphology is similar to that of crystalline nanowires commonly observed in P3HT homopolymers[32] and P3HT rod−coil diblock copolymers.[57] Together with the XRD measurements, these AFM images show that diblock copolymers self-assemble into a crystalline nanostructure. Previous AFM studies of crystalline nanowires from P3HT of a similar molecular weight to the P3HT in the present diblocks revealed a significantly narrower nanowires,[58] less than 15 nm in width compared to domains of 20 nm observed in the diblocks. This suggests that the PFO and PFBT blocks assemble around the nanowires, increasing the average size and distance between the nanowires. Furthermore, thin films of P3HT homopolymer matching the molecular weight of the P3HT block in the BCP films and processed under similar conditions show crystallinity but not periodic nanoscale domains (Supporting Information). This discrepancy indicates that BCP phase separation may increase the kinetics for the formation of laterally periodic nanostructures.

Structure of Diblock Copolymers in the Melt State. In contrast to AFM, which is only useful for characterizing the surface structure of a film, SAXS measurements reveal structural details throughout the thickness of a sample. SAXS traces show peaks corresponding to P3HT crystallites and lamellar domains in the diblock copolymer samples (Figure 8). For P3HT-*b*-PFO, no peaks are observed at temperatures above 190 °C after cooling from 250 °C, but two peaks emerge below 190 °C. Both peaks are thermally reversible and appear within a 5 °C window during cooling, as seen in Figure 8. Similar peaks are present in the SAXS traces for P3HT-*b*-PFBT powder samples. Above 200 °C no peaks are observed, but on cooling to 180 °C a P3HT crystal peak emerges along with a low-angle peak. The low-angle peak is weaker than that for P3HT-*b*-PFO but can be clearly resolved, and the peak disappears and reappears as the temperature is cycled. The lower intensity in the low-angle peak observed for P3HT-*b*-PFBT relative to P3HT-*b*-PFO may be due to the higher content of P3HT homopolymer impurity in the former.

Thus, the diblock copolymer samples undergo a structural transition on cooling below the crystallization temperature that results in nanoscale, crystalline domains throughout the bulk samples, not just in thin films or at the surface. A domain size can be calculated from $d = 2\pi/q^*$, where d is the lamellar spacing and q^* the position of the peak low-angle peak (0.025 and 0.023 $Å^{-1}$ for P3HT-*b*-PFO and P3HT-*b*-PFBT, respectively) to give a spacing of approximately 25 and 27 nm for P3HT-*b*-PFO and P3HT-*b*-PFBT, respectively. These numbers are close to the values for the domain spacing observed in the AFM images of diblock copolymer thin films and significantly larger than previously reported for pure P3HT nanowires (13.5 and 15.0 nm for 10.5 and 11.7 kg/mol P3HT, respectively).[58]

Analysis of the temperature dependent SAXS data shows that nanostructure formation in the diblock copolymers is coincident with the crystallization of P3HT. The SAXS crystallization transition can be evaluated from a plot of the inverse primary peak intensity versus the inverse temperature (Figure 9). As shown in the cooling scans, two scattering peaks appear concurrently, within a 5 °C temperature range. The transitions are much sharper on cooling; on heating, both transitions occur gradually at first, possibly due to the preferential melting of smaller crystallites or the disappearance of domains at lower temperatures. Nevertheless, both occur within similar temperature ranges on

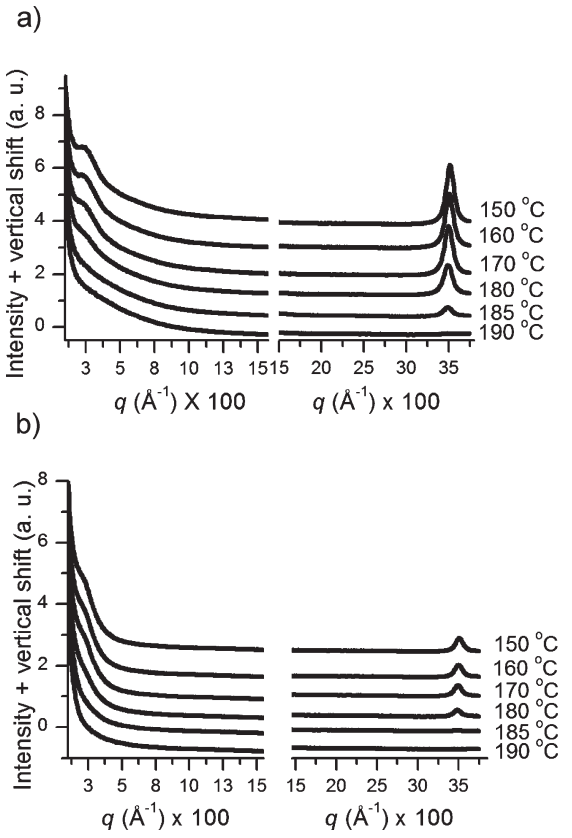

Figure 8. Small-angle X-ray scattering traces for (a) P3HT-*b*-PFO and (b) P3HT-*b*-PFBT measured at 8 keV (left axes) and 16 keV (right axes) on cooling from an annealing temperature of 250 °C.

cooling, and both transitions are shifted by approximately 20 °C on heating compared with cooling. The low-angle peak in diblock samples is only observed upon crystallization of P3HT, and no higher order peaks are present as is typical for self-assembled BCP nanostructures,[59] including some conjugated BCPs.[60] The polydispersity of the samples may preclude the formation of well-defined domains with long-range order, and the long-range ordering observed in polymer thin films could be indicative of nanostructuring influenced in part by interfacial effects that are less prominent in bulk samples. These interfacial effects may also account for the slower kinetics for self-assembly observed in polymer thin films compared with bulk polymer samples.

Previous reports on P3HT homopolymer films have found similar small-angle scattering traces, even in P3HT polymers with molecular weights as low as 2 kDa.[58,61] Therefore, both the SAXS and AFM data suggest that diblock copolymers self-assemble into crystalline nanofibrils or nanowires similar to those observed in P3HT. However, the presence of a PFO or PFBT block in the diblocks gives rise to BCP phase separation in addition to crystallization and nanowire formation. AFM and SAXS measurements indicate that the second polymer block increases the size and spacing between crystalline nanowires. In contrast to microphase segregation of coil−coil block copolymers,[59] phase separation accompanies nanowire formation and is driven by crystallization of the P3HT polymer block.

Conclusions

All-conjugated diblock copolymers can be synthesized using a two-step procedure that involves both GRIM and Suzuki polymerizations, followed by solvent extraction and column chromatography. The diblock copolymers produced in this study were

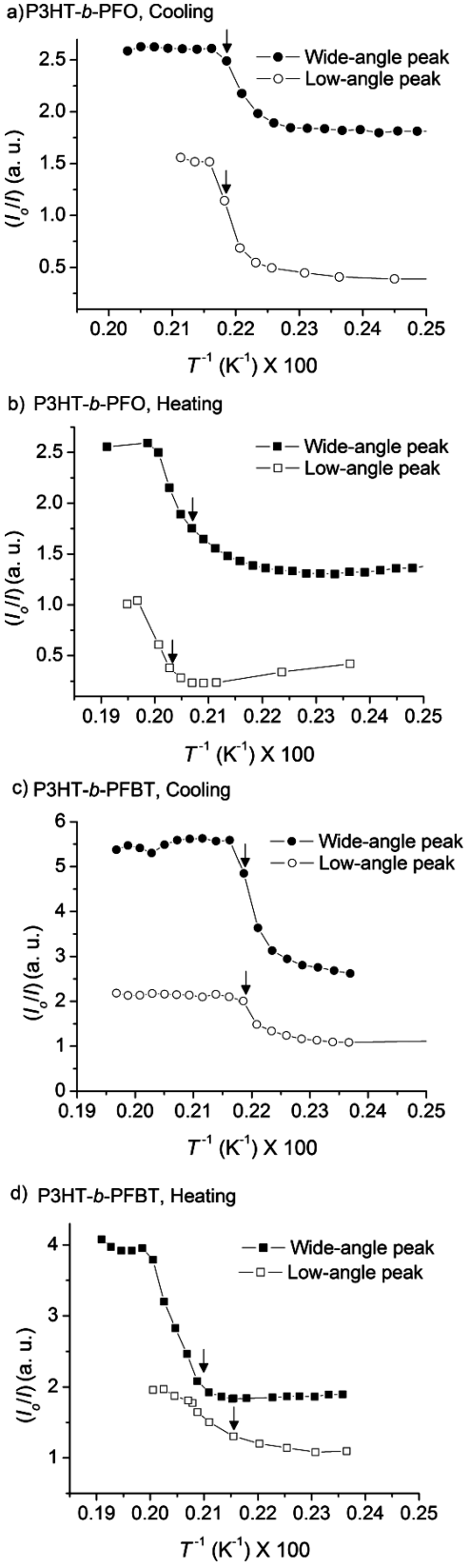

Figure 9. Inverse normalized intensity of peak heights in the vicinity of the order−disorder and crystallization transitions. Peak intensities are measured at 0.0252 and 0.348 Å^{-1} for P3HT-*b*-PFO and at 0.0232 and 0.351 Å^{-1} for P3HT-*b*-PFBT. The arrows mark the approximate positions for the start of a transition.

characterized using a combination of ^{1}H NMR, SEC−MALLS, and SEC−UV/vis to quantify the absolute molecular weight,

polymer compositions, and amount of homopolymer impurity. Our method for quantifying the amount of conjugated polymer impurities can be applied to conjugated BCPs in which the constituent polymer blocks have sufficiently different absorption spectra.

AFM measurements revealed the presence of periodic nanostructured domains in all-conjugated diblock copolymer thin films. These domains appeared only after extended solvent annealing and showed some long-range order. Analysis of temperature dependent SAXS data revealed simultaneous crystallization and nanostructure formation in powder diblock copolymer samples. This suggests that the diblock copolymers self-assemble into nanoscale domains due to crystallization of P3HT and incompatibility of the polymer blocks.

Crystallinity is a prerequisite for achieving organic materials with good mobilities for organic electronic applications, and the all-conjugated BCPs studied self-assemble into crystalline, nanoscale domains. The attachment of a second conjugated polymer block does not disrupt the crystallinity of P3HT, and periodic nanostructures can be formed both in thin films and in powder samples. All-conjugated diblock copolymers represent promising materials for controlling and tailoring the morphology of organic semiconductor systems, and the general approach presented here can be used to create tunable BCP organic active layers with nanoscale phase-separated p- and n-type regions.

Acknowledgment. R.V. acknowledges financial support from the Welch Foundation (Grant No. C-1750), the Louis Owen Foundation, and the Rice University School of Engineering start-up funds. Use of the Center for Nanoscale Materials was supported by the U.S. Department of Energy, Office of Science, Office of Basic Energy Sciences, under Contract DEAC02-06-CH11357. A portion of this research was conducted at the Center for Nanophase Materials Sciences, which is sponsored at Oak Ridge National Laboratory by the Division of Scientific User Facilities, U.S. Department of Energy. Use of the National Synchrotron Light Source, Brookhaven National Laboratory, was supported by the U.S. Department of Energy, Office of Science, Office of Basic Energy Sciences, under Contract No. DE-AC02-98CH10886.

Supporting Information Available: AFM images, small-angle X-ray scattering traces, DSC and TGA data, NMR spectra, and derivation of mathematical relationship between absorbance ratios and polymer composition and impurity.This material is available free of charge via the Internet at http://pubs.acs.org.

References and Notes

(1) Krebs, F. C.; Gevorgyan, S. A.; Alstrup, J. *J. Mater. Chem.* **2009**, *19* (30), 5442–5451.
(2) Zhan, X.; Zhu, D. *Polym. Chem.* **2010**, *1* (4), 409–419.
(3) Zaumseil, J.; Sirringhaus, H. *Chem. Rev.* **2007**, *107* (4), 1296–1323.
(4) D'Andrade, B. W.; Forrest, S. R. *Adv. Mater.* **2004**, *16* (18), 1585–1595.
(5) Thomas, S. W. I.; Joly, G. D.; Swager, T. M. *Chem. Rev.* **2007**, *107*, 1339–1386.
(6) Tang, C. W. *Appl. Phys. Lett.* **1986**, *48*, 183–185.
(7) Thompson, B. C.; Fréchet, J. M. J. *Angew. Chem., Int. Ed.* **2008**, *47* (1), 58–77.
(8) Dennler, G.; Scharber, M. C.; Brabec, C. J. *Adv. Mater.* **2009**, *21* (13), 1323–1338.
(9) Forrest, S. R. *MRS Bull.* **2005**, *30*, 28–32.
(10) Hoppe, H.; Sariciftci, N. S. *J. Mater. Chem.* **2006**, *16* (1), 45–61.
(11) Geffroy, B.; Roy, P. l.; Prat, C. *Polym. Int.* **2006**, *55* (6), 572–582.
(12) Bates, F. S.; Fredrickson, G. H. *Phys. Today* **1999**, *52*, 32–38.
(13) Park, C.; Yoon, J.; Thomas, E. L. *Polymer* **2003**, *44*, 6725–6760.
(14) Darling, S. B. *Prog. Polym. Sci.* **2007**, *32*, 1152–1204.
(15) Darling, S. B. *Energy Environm. Sci.* **2009**, *2*, 1266–1273.
(16) Segalman, R. A.; McCulloch, B.; Kirmayer, S.; Urban, J. J. *Macromolecules* **2009**, *42*, 9205–9216.
(17) Botiz, I.; Darling, S. B. *Mater. Today* **2010**, *13* (5), 42–51.
(18) Sommer, M.; Huettner, S.; Thelakkat, M. *J. Mater. Chem.* **2010**, *20* (48), 10788–10797.
(19) Sun, S. S.; Zhang, C.; Ledbetter, A.; Choi, S.; Seo, K.; Bonner, C. E.; Drees, M.; Sariciftci, N. S. *Appl. Phys. Lett.* **2007**, *90*, 043117.
(20) Xiao, X.; Fu, Y.; Sun, M.; Li, L.; Bo, Z. *J. Polym. Sci., Part A: Polym. Chem.* **2007**, *45* (12), 2410–2424.
(21) Veenstra, S. C.; Loos, J.; Kroon, J. M. *Prog. Photovolt.: Res. Appl.* **2007**, *15*, 727–740.
(22) McNeill, C. R.; Halls, J. J. M.; Wilson, R.; Whiting, G. L.; Berkebile, S.; Ramsey, M. G.; Friend, R. H.; Greenham, N. C. *Adv. Funct. Mater.* **2008**, *18* (16), 2309–2321.
(23) Kietzke, T.; Hörhold, H.-H.; Neher, D. *Chem. Mater.* **2005**, *17*, 6532–6537.
(24) Koetse, M. M.; Sweelssen, J.; Hoekerd, K. T.; Schoo, H. F. M.; Veenstra, S. C.; Kroon, J. M.; Yang, X.; Loos, J. *Appl. Phys. Lett.* **2006**, *88* (8), 083504.
(25) McNeill, C. R.; Greenham, N. C. *Adv. Mater.* **2009**, *21* (38−39), 3840–3850.
(26) Granstrom, M.; Petritsch, K.; Arias, A. C.; Lux, A.; Andersson, M. R.; Friend, R. H. *Nature* **1998**, *395* (6699), 257–260.
(27) McNeill, C. R.; Abrusci, A.; Zaumseil, J.; Wilson, R.; McKiernan, M. J.; Burroughes, J. H.; Halls, J. J. M.; Greenham, N. C.; Friend, R. H. *Appl. Phys. Lett.* **2007**, *90* (19), 193506–3.
(28) Arias, A. C.; MacKenzie, J. D.; Stevenson, R.; Halls, J. J. M.; Inbasekaran, M.; Woo, E. P.; Richards, D.; Friend, R. H. *Macromolecules* **2001**, *34* (17), 6005–6013.
(29) McNeill, C. R.; Watts, B.; Thomsen, L.; Ade, H.; Greenham, N. C.; Dastoor, P. C. *Macromolecules* **2007**, *40* (9), 3263–3270.
(30) Kim, Y.; Cook, S.; Choulis, S. A.; Nelson, J.; Durrant, J. R.; Bradley, D. D. C. *Chem. Mater.* **2004**, *16* (23), 4812–4818.
(31) Scherf, U.; Gutacker, A.; Koenen, N. *Acc. Chem. Res.* **2008**, *41* (9), 1086–1097.
(32) Osaka, I.; McCullough, R. D. *Acc. Chem. Res.* **2008**, *41* (9), 1202–1214.
(33) Wu, P.-T.; Ren, G.; Li, C.; Mezzenga, R.; Jenekhe, S. A. *Macromolecules* **2009**, *42*, 2317–2320.
(34) Iovu, M. C.; Sheina, E. E.; Gil, R. R.; McCullough, R. D. *Macromolecules* **2005**, *38*, 8649–8656.
(35) Yokozawa, T.; Adachi, I.; Miyakoshi, R.; Yokoyama, A. *High Perfom. Polym.* **2007**, *19*, 684–699.
(36) Zhang, Y.; Tajima, K.; Hirota, K.; Hashimoto, K. *J. Am. Chem. Soc.* **2008**, *130*, 7812–7813.
(37) Ouhib, F.; Khoukh, A.; Ledeuil, J.-B.; Martinez, H.; Desbrieres, J.-B.; Dagron-Lartigau, C. *Macromolecules* **2008**, *41*, 9736–9743.
(38) Zhang, Y.; Tajima, K.; Hashimoto, K. *Macromolecules* **2009**, *42*, 7008–7015.
(39) Ouhib, F.; Khoukh, A.; Ledeuil, J.-B.; Martinez, H.; Desbrieres, J.; Dagron-Lartigau, C. *Macromolecules* **2008**, *41* (24), 9736–9743.
(40) Miyanishi, S.; Zhang, Y.; Tajima, K.; Hashimoto, K. *Chem. Commun.* **2010**, *46* (36), 6723–6725.
(41) Javier, A. E.; Varshney, S. R.; McCullough, R. D. *Macromolecules* **2010**, *43* (7), 3233–3237.
(42) Huang, L.; Wu, S.; Qu, Y.; Geng, Y.; Wang, F. *Macromolecules* **2008**, *41* (22), 8944–8947.
(43) Park, J. Y.; Koenen, N.; Ponnapati, R.; Scherf, U.; Advincula, R. *Macromolecules* **2008**, *41* (16), 6169–6175.
(44) Tu, G.; Li, H.; Forster, M.; Heiderhoff, R.; Balk, L. J.; Sigel, R.; Scherf, U. *Small* **2007**, *3* (6), 1001–1006.
(45) Ohshimizu, K.; Shibasaki, Y.; Komura, M.; Nakajima, K.; Ueda, M. *Chem. Lett.* **2007**, *36* (6), 742–743.
(46) Zhang, X.; Tian, H.; Liu, Q.; Wang, L.; Geng, Y.; Wang, F. *J. Org. Chem.* **2006**, *71*, 4332–4335.
(47) Prillman, S.; Colvin, V., *TappminModeTM - Atomic Force Microscopy Manual*. In Colvin, V., Ed.; Rice University: Houston, TX, 1997; Vol. *1.1* (http://nanonet.rice.edu/manuals/afm.html).
(48) Herguth, P.; Jiang, X.; Liu, M. S.; Jen, A. K.-Y. *Macromolecules* **2002**, *35*, 6094–6100.
(49) Cheng, Y.-J.; Yang, S.-H.; Hsu, C.-S. *Chem. Rev.* **2009**, *109*, 5868–5923.
(50) Campbell, A. J.; Bradley, D. D. C.; Antoniadis, H. *Appl. Phys. Lett.* **2001**, *79* (14), 2133–2135.

(51) Malik, S.; Nandi, A. K. *J. Polym. Sci., Part B: Polym. Phys.* **2002**, *40* (18), 2073–2085.
(52) Chen, T.-A.; Wu, X.; Rieke, R. D. *J. Am. Chem. Soc.* **1995**, *117*, 233–244.
(53) Kawana, S.; Durrell, M.; Lu, J.; Macdonald, J. E.; Grell, M.; Bradley, D. D. C. *Polymer* **2002**, *43*, 1907–1913.
(54) Botiz, I.; Darling, S. B. *Macromolecules* **2009**, *42* (21), 8211–8217.
(55) Boudouris, B. W.; Frisbie, C. D.; Hillmyer, M. A. *Macromolecules* **2007**, *41* (1), 67–75.
(56) Zhang, Y.; Tajima, K.; Hashimoto, K. *Macromolecules* **2009**, *42* (18), 7008–7015.
(57) Iovu, M. C.; Jeffries-El, M.; Zhang, R.; Kowalewski, T.; McCullough, R. D. *J. Macromol. Sci.: Pure Appl. Chem.* **2006**, *43* (12), 1991–2000.
(58) Zhang, R.; Li, B.; Iovu, M. C.; Jeffries-El, M.; Sauvé, G.; Cooper, J.; Jia, S.; Tristram-Nagle, S.; Smilgies, D. M.; Lambeth, D. N.; McCullough, R. D.; Kowalewski, T. *J. Am. Chem. Soc.* **2006**, *128* (11), 3480–3481.
(59) Hamley, I. W., *The Physics of Block Copolymers*. Oxford University Press: Oxford, U.K., 1998.
(60) Olsen, B. D.; Segalman, R. A. *Macromolecules* **2006**, *39*, 7078–7083.
(61) Canetti, M.; Bertini, F.; Scavia, G.; Porzio, W. *Eur. Polym. J.* **2009**, *45* (9), 2572–2579.